JACS
JOURNAL OF THE AMERICAN CHEMICAL SOCIETY

ARTICLE

pubs.acs.org/JACS

Distinctive Attributes of β-Lactam Target Proteins in *Acinetobacter baumannii* Relevant to Development of New Antibiotics

Seungil Han,* Nicole Caspers, Richard P. Zaniewski, Brian M. Lacey, Andrew P. Tomaras, Xidong Feng, Kieran F. Geoghegan, and Veerabahu Shanmugasundaram

Pfizer Worldwide Research, Eastern Point Road, Groton, Connecticut 06340, United States

Supporting Information

ABSTRACT: Multi-drug-resistant forms of the Gram-negative pathogen *Acinetobacter baumannii* are an emerging threat to human health and further complicate the general problem of treating serious bacterial infections. Meeting this challenge requires an improved understanding of the relationships between the structures of major therapeutic targets in this organism and the activity levels exhibited against it by different antibiotics. Here we report the first crystal structures of *A. baumannii* penicillin-binding proteins (PBPs) covalently inactivated by four β-lactam antibiotics. We also relate the results to kinetic, biophysical, and computational data. The structure of the class A protein PBP1a was solved in apo form and for its covalent conjugates with benzyl penicillin, imipenem, aztreonam, and the siderophore-conjugated monocarbam MC-1. It included a novel domain genetically spliced into a surface loop of the transpeptidase domain that contains three conserved loops. Also reported here is the first high-resolution structure of the *A. baumannii* class B enzyme PBP3 in apo form. Comparison of this structure with that of MC-1-derivatized PBP3 of *Pseudomonas aeruginosa* identified differences between these orthologous proteins in *A. baumannii* and *P. aeruginosa*. Thermodynamic analyses indicated that desolvation effects in the PBP3 ligand-binding sites contributed significantly to the thermal stability of the enzyme−antibiotic covalent complexes. Across a significant range of values, they correlated well with results from studies of inactivation kinetics and the protein structures. The structural, biophysical, and computational data help rationalize differences in the functional performance of antibiotics against different protein targets and can be used to guide the design of future agents.

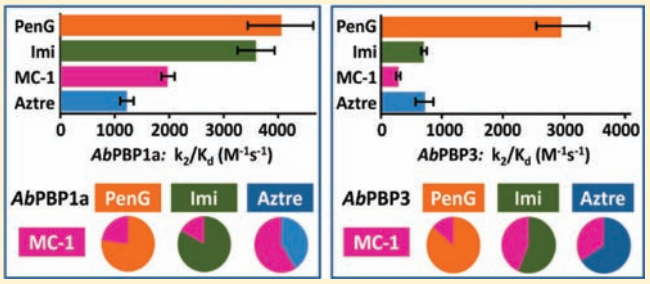

INTRODUCTION

Reports in the scientific literature increasingly refer to a crisis in the treatment of infectious diseases, especially those caused by Gram-negative pathogens.[1,2] While new multi-drug-resistant strains are emerging at an alarming rate, the development of antibiotics that would mitigate their threat is now seriously attenuated.[2] Economic and even legal elements have their roles in this difficulty,[3] but the principal cause may reside in the weakness of the classical paradigm for the discovery of new antibacterial agents. This typically consists of alternating rounds of screening for microbicidal activity and medicinal chemical optimization of lead compounds until an adequate level of antibiotic effect is established. As an attractively direct and relatively uncomplicated approach, it remains in use after a generally disappointing foray into target-specific discovery efforts sparked by the onset of genomic sequencing in the 1990s.[4]

β-Lactam antibiotics disrupt cell-wall synthesis in Gram-negative bacteria by covalently inactivating members of a family of enzymes known as penicillin-binding proteins (PBPs). Activity against a broad spectrum of pathogens is desirable in these compounds, but functionally comparable orthologs of an individual PBP from different pathogens may have different sensitivities to an antibiotic. Recognizing and accommodating these variations in the target proteins should be an essential aspect of modern antibiotic discovery, and appears to be a step toward meeting the increasing challenge represented by multi-drug-resistant Gram-negatives.[2,5]

The greater part of research interest has gone to characterizing PBPs from the most clinically prominent Gram-negative bacilli including *Pseudomonas aeruginosa* and *Klebsiella pneumoniae*, but *Acinetobacter baumannii* continues to grow in significance as an additional threat to human health.[6,7] Drug resistance is growing in this organism at an alarming rate,[8] and its key target proteins need to be characterized in detail to promote ongoing efforts to target it effectively with β-lactams.

PBPs work in the periplasm to assemble the Gram-negative bacterial cell wall, a cross-linked peptidoglycan matrix that forms an essential envelope around the inner cytoplasmic membrane and helps to maintain the structural integrity of the cell. High-molecular weight class A PBPs (PBP1a and PBP1b) are bifunctional enzymes that perform both transglycosylase and transpeptidase functions.[9]

Received: September 19, 2011
Published: November 03, 2011

Class B high molecular-weight PBPs perform only transpeptidase functions. At least six PBPs of *A. baumannii* have been detected by their ability to form covalent adducts with radiolabeled penicillin G.[10,11]

Access to these periplasmic targets is complicated by the existence of the outer membrane, which can exclude β-lactam-type antibiotics if the expression of specific porin channels is downregulated.[8] As a result, it is an attractive strategy to design Gram-negative antibacterial agents that traverse the outer membrane in a porin-independent manner. The "Trojan Horse" approach to solving this problem is inspired by awareness that bacteria secrete siderophores with prodigious affinity for iron in order to capture and accumulate this critical element. Iron is generally very poorly abundant in free form in host tissues. Specialized transport systems exist at the cell surface to perform the necessary uptake step by which chelated iron is brought into the cell.[12,13] Combining a siderophore mimic with a novel β-lactam antibiotic is a promising tactic for achieving porin-independent uptake of a therapeutic agent.[14−18]

This paper describes functional studies (both enzymatic and antimicrobial) of MC-1, a Trojan Horse agent of this kind, against *A. baumannii* and one each of its class A and class B PBPs. To date,[19] comparisons of the actions of MC-1 with those of classical β-lactam agents have been based mainly on direct measurements of antibacterial potency ($MIC_{50/90}$), leaving uncertainty as to the extent to which the target enzymes of *A. baumannii* differ in their structures from their more widely studied orthologs in *P. aeruginosa*. In this report, crystallographic analyses of PBP1a and PBP3 of *A. baumannii* allow direct comparisons of defined molecular structures. The new structures, together with associated biophysical and computational data, suggest potential strategies in medicinal chemistry to improve the potency of agents that target the emerging pathogenic threat of *A. baumannii*.

MATERIALS AND METHODS

Expression, Purification, and Crystallization of *A. baumannii* PBP1a (*Ab*PBP1a). A soluble form of *Ab*PBP1a (residues 26−739 preceded by an N-terminal His_6 tag and TEV cleavage site) was expressed by cloning the bacterial DNA into the pET28a vector (Novagen) by standard methods and overexpressing the recombinant product in *E. coli* BL21-Gold(DE3) grown in LB medium for 24 h at 37 °C. Selenomethionine (SeMet)-substituted *Ab*PBP1a was expressed in M9 minimal medium. The resulting cell paste was suspended in 10 volumes (w/v) of buffer A (25 mM Tris, 400 mM NaCl, 5% glycerol, 10 mM imidazole, pH 8.0). Protease inhibitors (1 tablet of complete EDTA free protease inhibitor cocktail per 50 mL, Roche Applied Science) and benzonase (10 μL, Sigma) were added to the suspension. Cells were lysed with one pass through a microfluidizer (18 000 psi). The lysate was clarified by centrifugation at 4 °C for 45 min at 30 000*g* in a Sorvall SLA-1500 rotor. The extracted supernatant was decanted and added to 15 mL Ni-NTA Superflow (Qiagen) that had been equilibrated in buffer A. The *Ab*PBP1a protein was batch-bound to the resin for 2 h at 4 °C with rocking. The resin was poured into a gravity flow column and washed with 10 column volumes of buffer A + 1.5 M NaCl followed by 10 column volumes of buffer A + 20 mM imidazole. The protein was eluted with buffer A + 250 mM imidazole. The Ni-NTA eluate was diluted 8-fold with buffer B (25 mM Tris, 5% glycerol, pH 8.0) and loaded onto 5 mL HiTrap Q and 5 mL HiTrap SP columns connected in series. The columns were washed with 50 mM NaCl in buffer B, and the Q column was removed. Bound protein was then eluted from the SP column with a step gradient in increments of 100 mM NaCl. *Ab*PBP1a was eluted in 400 mM NaCl. Trypsin was added in a molar ratio of 1:20 trypsin/*Ab*PBP1a, and the reaction was incubated for 1 h at room temperature. The reaction was treated with 1 mM EDTA, and the trypsin-digested protein was purified over the HiTrap Q and HiTrap SP columns as before. The *Ab*PBP1a protein was eluted as a single peak from the SP column at 400 mM NaCl, and then concentrated and loaded onto a Superdex 200 16/60 column equilibrated in 25 mM Tris, 1 M NaCl, 10% glycerol. The resulting protein peak was concentrated to 15 mg/mL with a 30 kDa MWCO Amicon Ultra. Aliquots were snap frozen in liquid nitrogen and stored at −80 °C until they were used for crystallization.

Crystals of apo *Ab*PBP1a and of its Se-Met-substituted form were grown by hanging drop vapor diffusion at room temperature. Equal volumes of 15 mg/mL protein were mixed with reservoir solution containing 25% PEG monomethylether 5000, 0.1 M MES pH 6.5, 0.1 M sodium acetate. Cocrystals of the complex with MC-1 were grown in the same conditions using protein at 13 mg/mL with 1 mM compound. For other inhibitor complexes, cocrystallization was achieved with reservoir solution containing 30% PEG monomethylether 2000, 0.1 M Mes, 0.1 M sodium acetate, pH 6.5. Optimized cocrystals complexed with benzyl penicillin (Pen G) and imipenem were obtained using 0.02 M betaine hydrochloride and β-nicotinamide adenine dinucleotide, respectively. Crystals were cryoprotected in 20% glycerol in reservoir solution prior to freezing in liquid nitrogen.

***A. baumannii* PBP3 (*Ab*PBP3) Cloning, Expression, Purification, and Crystallization.** DNA encoding the periplasmic domain of *Ab*PBP3 (residues 64−609) fused to an N-terminal His_6 tag was cloned into the pET28 vector (Novagen), and protein was produced in *E. coli* BL21 (Gold) cells grown in autoinduction medium (Novagen) for 24 h at 25 °C. The *E. coli* cell pellet was resuspended in 10 volumes (w/v) of 25 mM Tris, 400 mM NaCl, 10 mM imidazole, 10% glycerol, 0.1% CHAPS, pH 8.0. Protease inhibitors (1 tablet of complete EDTA free protease inhibitor cocktail per 50 mL) and benzonase (10 μL) were added to the suspension. Cells were lysed with one pass through the microfluidizer (18 000 psi) and the lysate was clarified by centrifugation at 4 °C for 45 min at 30 000*g* in a Sorvall SLA-1500 rotor. The extracted supernatant was decanted and added to 15 mL Ni-NTA Superflow (Qiagen) previously equilibrated in buffer A (25 mM Tris, 400 mM NaCl, 50 mM imidazole, 10% glycerol, pH 8.0). The protein was batch-bound to the resin for 2 h at 4 °C with rocking. The resin slurry was poured into an XK column and then washed on an AKTA purifier with buffer A until A_{280} reached baseline. The protein was eluted with 25 mM Tris, 400 mM NaCl, 200 mM imidazole, 10% glycerol, pH 8.0. The eluted peak was diluted 8-fold with buffer B (25 mM Tris, 10% glycerol, pH 8.0) to lower the salt concentration to 50 mM. The protein was loaded onto two 5 mL HiTrap SP HP columns in series previously equilibrated in buffer B and then was eluted with a gradient to 500 mM NaCl over 20 column volumes. Peak fractions were pooled and concentrated to 10 mL, and then loaded onto a Superdex 200 HR 16/60 column (GE Healthcare) equilibrated in 25 mM Tris, 200 mM NaCl, 10% glycerol, pH 8.0. The peak fractions were pooled and concentrated to 15 mg/mL with an Amicon Ultra 30 kDa MWCO centrifugal concentrator. Protein aliquots were snap frozen in liquid nitrogen and stored at −80 °C. Crystals of apo *Ab*PBP3 were obtained by hanging drop vapor diffusion at 4 °C. Equal volumes of 10 mg/mL protein were mixed with reservoir solution containing 10% PEG 4000, 0.1 M Tris pH 7.5. Crystals were cryoprotected in 20% glycerol in reservoir solution prior to freezing in liquid nitrogen.

Structure Determination. X-ray diffraction data were collected at the 17-ID beamline of the Advanced Photon Source of the Argonne National Laboratory on a Pilatus detector and at beamline BL17U of the Shanghai Synchrotron Radiation Facility. Data were processed using the HKL2000 software suite.[20] The *Ab*PBP1a structure was solved by SAD phasing using SHARP/autoSHARP.[21] The model was built using ARP/wARP[22] and COOT[23] and then refined with autoBUSTER.[24] The refined *Ab*PBP1a-apo structure was then used as a starting model for antibiotic complexes of the protein. The structure of apo-*Ab*PBP3 was

solved by molecular replacement methods with the CCP4 version of PHASER,[25] using *P. aeruginosa* PBP3 (*Pa*PBP3) (PDB code: 3PBN) as a search model. After molecular replacement, maximum likelihood-based refinement of the atomic position and temperature factors were performed with autoBUSTER,[24] and the atomic model was built with the program COOT.[23] The stereochemical quality of the final model was assessed with PROCHECK.[26] Crystallographic statistics for the final models are shown in Table S2. Figures were prepared with PYMOL (www.pymol.org).

Minimal Inhibitory Concentration (MIC). A recent clinical isolate of multiple drug-resistant *A. baumannii* (no. 1733−09) was assayed using broth microdilution following Clinical and Laboratory Standards Institute (CLSI) guidelines for antimicrobial susceptibility testing.

***Ab*PBP1a Competitive Binding Assay.** Solutions (200 μM) of β-lactam compounds were serially diluted 2-fold in phosphate buffered saline (PBS) so that 25 μL assays that each included 5 μL of one β-lactam dilution contained β-lactam at concentrations ranging from 40 to 0.039 μM. The β-lactams were assayed at 11 nonzero concentrations alongside a zero compound control. A 5 μL aliquot of each compound dilution was first combined with 5 μL of 3 μM Bocillin FL (Invitrogen) so that the final Bocillin FL concentration in 25 μL would be 0.6 μM. The assay was then started by adding 15 μL of a 20 μg/mL solution of *Ab*PBP1a in PBS. Each assay therefore contained 300 ng of *Ab*PBP1a. The mixture was incubated at 35 °C for 20 min, after which the reaction was terminated by adding 25 μL of 2× Laemmli sample buffer. The samples were incubated in a boiling water bath for 3 min and then centrifuged at 14 000 rpm (3 min) in an Eppendorf centrifuge. A 10 μL sample from each assay was loaded onto a 10% NuPAGE gel (Invitrogen) run with NuPAGE Mes buffer at 150 V for 75 min. The gel was washed briefly in deionized H_2O and then scanned with a Storm 860 phosphoimager (Molecular Dynamics) using an excitation wavelength of 450 nm and an emission wavelength of 520 nm. EC_{50} for each β-lactam assayed was the concentration at which it caused a 50% reduction in the binding of Bocillin FL to the PBP.

Rapid Quenched Flow. Rates of acylation of *Ab*PBP3 and *Ab*PBP1a by β-lactams were determined using a RQF-3 Rapid Quench-Flow instrument (KinTek) as described.[27]

Thermal Stability Assay. Thermal shift assays were conducted in the iCycler iQ Real Time Detection System (Bio-Rad) originally designed for PCR. The instrument contained a heating/cooling device for accurate temperature control and a CCD detector for simultaneous imaging of fluorescence changes in microplate wells. A protein concentration of 7 μM was used with the addition of 100 μM test compound and SYPRO orange dye (Invitrogen) added to a final concentration that was 1000-fold diluted relative to the supplied "5000× concentrate". The plate was heated from 25 to 90 °C at a rate of 1.0 °C/min. Excitation and emission wavelengths were 490 and 530 nm, respectively.

LC-MS of Limited Trypsin-Catalyzed Proteolysis of *Ab*PBP1a. The product of limited trypsin-catalyzed proteolysis of recombinant *Ab*PBP1a was initially subjected to LC-MS using an Agilent 1100 HPLC system operating at a flow rate of 0.02 mL/min and connected to an Applied Biosystems QSTAR XL hybrid (quadrupole/quadrupole/time-of-flight) mass spectrometer equipped with a TurboIonSpray source and running under Analyst QS software. A Vydac C4 column (100 mm × 0.3 mm; type 214MS5.310) was used with solvents as follows: A, 0.1% formic acid; B, 0.1% formic acid in acetonitrile. The gradient used was: 0−1 min, 1.6% B isocratic; 1−45 min, 1.6−70% B; 45−46 min, 70−100% B. Additional peptide mapping was conducted on a Thermo Scientific LTQ spectrometer as described.[28]

LC-MS Competition Experiments. *Ab*PBP1a and *Ab*PBP3 were prepared at 7.1 μM in Dulbecco's phosphate-buffered saline lacking magnesium and calcium, pH 7.2 (Sigma D8537). Solutions of Pen G, imipenem, aztreonam, and MC-1 were prepared from their solid forms, initially in DMSO at known concentrations near 1 mg/mL and subsequently diluted with PBS. Exposure of compounds to the aqueous buffer prior to mixing with protein was kept to a minimum. Each protein (3.55 μM final concentration) was mixed at room temperature (about 24 °C) with single or mixed compounds (7.1 μM final concentration of each compound), and incubated at room temperature for 1 h before being placed in an autosampler queue at 4 °C for LC-MS. For competition experiments using two, three, or four compounds, compounds were mixed together before being added to the protein. LC-MS was performed on the QSTAR XL system described above, but with a steeper acetonitrile gradient: 0−1 min, 1.6% B isocratic; 1−22.5 min, 1.6−75% B; 22.5−23 min, 75−100% B. Mass spectra were acquired over the range m/z 400−2000 and deconvoluted using the Bayesian Protein Reconstruction tool from Analyst QS 1.1. Relative reactivities of compounds with each PBP were calculated from peak heights in deconvoluted mass spectra.

Scheme 1. Chemical Structures of Antibiotics Relevant to This Study

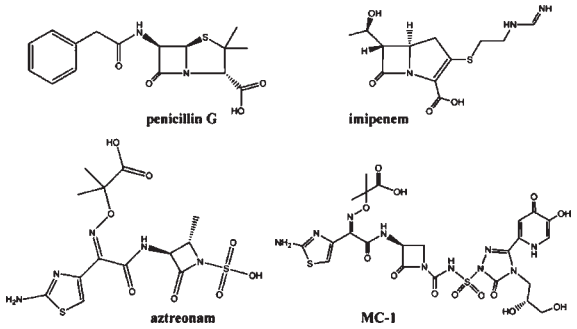

WaterMap Calculations. WaterMap[29−32] calculations were performed on the apo structure of *Ab*PBP1a and on the four ligand-complex crystal structures (Pen G, imipenem, aztreonam, MC-1). Initial structures were prepared with the Protein Preparation Wizard in Maestro 9.0 (Schrödinger), and all crystallographic water molecules were deleted. The protein was solvated in a TIP4P water box extending at least 5 Å beyond the protein in all directions. The default Desmond relaxation protocol was applied with the OPLS2005 force field,[33−35] which involved successive stages of minimization and heating. A 2 ns production MD simulation with positional restraints on the protein non-hydrogen atoms was performed following the relaxation. Water molecules from each of the approximately 2000 equally spaced snapshots from the simulation were clustered to form hydration sites. The enthalpy was computed from the average nonbonded energy of each hydration site. The excess entropy was computed by numerically integrating a local expansion of spatial and orientational correlation functions. The enthalpy (ΔH) relative to bulk water was calculated for water molecules within each hydration site using the OPLS-AA molecular mechanics force field. The degree of ordering of water molecules relative to bulk water determined the entropy term ($-T\Delta S$), for which the entropy of bulk water was defined as $S_{bulk} = 0$. The average entropy, enthalpy, and free energy were computed for each hydration site along with the occupancy of each hydration site and the average number of hydrogen bonds with protein polar atoms and other water molecules.[29] The default scoring function was used for scoring the ligands.

Data Deposition. New X-ray structures have been deposited in the Protein Data Bank with the accession codes 3UDF, 3UDI, 3UDX, 3UE0, 3UE1, and 3UE3.

RESULTS AND DISCUSSION

Recombinant proteins corresponding to a soluble fragment of *Ab*PBP1a and the periplasmic domain of *Ab*PBP3 were studied as representative targets for β-lactam action in *A. baumannii*.

The compound constant k_2/K_d, which reflects a compound's overall efficiency at inactivating an enzyme target, was derived against these proteins for three conventional β-lactams along with the hybrid metal-chelating/β-lactam agent MC-1 (Scheme 1). This value is directly proportional to the rate constant for the irreversible step of inactivation (acylation of active-site serine in the PBPs) and inversely proportional to the compound's dissociation constant from the protein target.

Stopped-flow mixing followed by mass spectrometry was used to gauge the extent of protein modification as a function of time, with compounds exhibiting the following order of efficiency (strongest to weakest) against *Ab*PBP1a: Pen G = imipenem > MC-1 > aztreonam (Figure 1A, bar graph). The range of values against PBP1a covered a spread of slightly more than 3-fold. Against *Ab*PBP3, Pen G was again the most efficient agent (Figure 1B, bar graph), outperforming the other three antibiotics by a factor of about 3.

From the independently measured values of k_2/K_d, predictions could then be made of the outcome of competitive experiments in which each PBP was exposed in a single mixing step to an equimolar concentration of MC-1 and one of the other three agents. The ratio of protein to each drug was 1:2. Competitive outcomes measured by electrospray/time-of-flight mass spectrometry agreed well with projections from the single-compound method. For *Ab*PBP1a (Figure 1A, pie chart), MC-1 slightly outperformed aztreonam but occupied just under 25% of the *Ab*PBP1a when competing with Pen G or imipenem. For *Ab*PBP3 (Figure 1B, pie chart), MC-1 competed weakly with Pen G but occupied a fraction close to 50% of the protein when competing with imipenem or aztreonam.

The results showed that MC-1 acylated two PBP targets of *A. baumannii* with efficiencies not greatly different from those exhibited by imipenem and aztreonam, two antibiotics for which there is considerable clinical experience. This is further confirmation that a compound with the special attributes of MC-1 is a viable agent when delivered to its target sites of action,[27] and allows continuing attention to focus on its delivery and uptake.

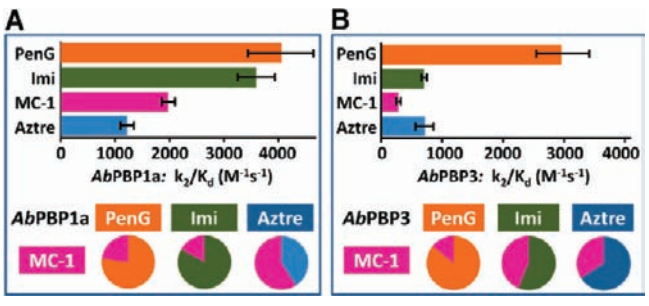

Figure 1. Independent and competitive analyses of (A) *Ab*PBP1a and (B) *Ab*PBP3 modification by β-lactam antibiotics. In each panel, the bar graph shows k_2/K_d values measured for benzyl penicillin (Pen G), imipenem (Imi), MC-1, and aztreonam (Aztre) by quenched-flow kinetic analysis and mass spectrometry. In each panel, the pie chart shows the result of competitive reactions with the target protein, in each case using MC-1 and one other compound. Occupancy ratios were measured by mass spectrometry. The ratio of protein/MC-1/competitor was 1:2:2.

We also gauged the ability of each of the four compounds to compete for *Ab*PBP1a with the covalent and fluorescent active-site probe Bocillin FL. The order of affinity for *Ab*PBP1a indicated by this study was Pen G and MC-1 > imipenem > aztreonam, with respective EC_{50} values (μM) of 0.44, 0.48, 0.89, and 1.68.

Antibacterial Activity. MIC measurements against *A. baumannii* were then obtained for the four test agents (Table 1), but the effect of β-lactamase action on the activities was a prime feature of the result. Imipenem performed best (MIC of 0.125−0.25 μg/mL), followed by MC-1 and aztreonam (both with MIC of 1−2 μg/mL), and Pen G was very much less effective. In the presence of the β-lactamase inhibitor tazobactam, all the test agents had MIC < 0.06 μg/mL against both strains.

Imipenem, the most effective agent of the four tested, is a carbapenem with an extended side chain at the C2 position. It exhibits a broad antibacterial spectrum, and is used primarily to combat penicillin- and cephalosporin-resistant bacteria.[36,37] Aztreonam is a monocyclic β-lactam (monobactam) bearing a 2-oxazetidine-1-sulfonic acid moiety that shows very high affinity for PBP3 of Gram-negative bacteria including *P. aeruginosa*.[38] MC-1 has already been shown to be highly efficacious against multiply drug-resistant *P. aeruginosa* and extended-spectrum β-lactamase-producing members of the *Enterobacteriaceae*.[19,27] To develop structural information that could be useful in refining the design of MC-1-related agents toward an optimized profile

Figure 2. Tryptic processing of recombinant PBP1a to yield a crystallizable protein. Sequence numbering follows residues 26−739 of the natural sequence of PBP1a (UniProt accession B2I0J9). Lower-case sequence is non-natural. Sequence in red was detected by mass spectrometry (both direct and by peptide mapping) of the crystallizable protein, and underlined sequence was resolved in the crystal structure of PBP1a.

Table 1. Antibiotic MIC Values against *Acinetobacter baumannii* Strain 1733-09

tazobactam (μg/mL)	aztreonam MIC (μg/mL)	aztreonam + tazobactam MIC (μg/mL)	imipenem MIC (μg/mL)	imipenem + tazobactam MIC (μg/mL)	Pen G MIC (μg/mL)	Pen G + tazobactam MIC (μg/mL)	MC-1 MIC (μg/mL)	MC-1 + tazobactam MIC (μg/mL)
0.5	1	<0.06	0.25	<0.06	32	<0.06	2	<0.06
2.0	1	<0.06	0.125	<0.06	16	<0.06	1	<0.06

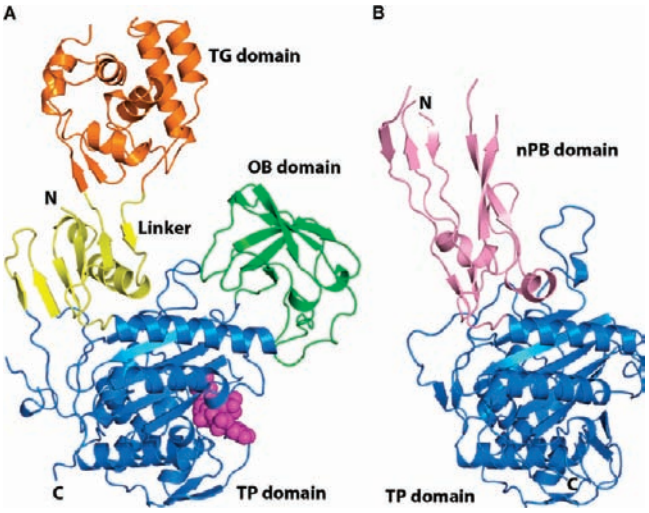

Figure 3. Overall structures of *Acinetobacter* PBP1a and PBP3. (A) Structure of *Ab*PBP1a complexed with MC-1. The bound MC-1 is shown as spheres. (B) The *Ab*PBP3 structure with N-terminal domain in pink and the C-terminal domain in blue.

including efficacy against *A. baumannii*, structural studies were next undertaken of *A. baumannii* PBP1a and PBP3.

Structure of *Ab*PBP1a. Despite an extensive effort with more than 80 different constructs, crystals could not be obtained directly from recombinant *Ab*PBP1a, and a method based on controlled proteolysis with trypsin was applied (see Materials and Methods for details). Trypsin treatment followed by chromatographic cleanup gave a form of the protein that could crystallize and was shown by mass spectrometry to consist of three major associated polypeptides. These were Lys27-Phe72, Lys129-Lys608, and Gln619-Lys736 (Figure 2).

The structure of *Ab*PBP1a was determined using phasing information from single-wavelength anomalous dispersion (SAD) data collected using a selenomethionine-substituted crystal and refined using a native data set to 1.7 Å resolution. The protein structure revealed by crystallography (Figure 3A) was in excellent agreement with the composition detected by mass spectrometry. *Ab*PBP1a derivatized with each of the compounds Pen G, imipenem, aztreonam, and MC-1 gave their respective crystal structures by the same protocol.

In *Ab*PBP1a, a class A PBP, the initial transmembrane helix is followed by an N-terminal transglycosylase (TG) domain connected through a β-rich linker to a C-terminal transpeptidase (TP) domain. Similar TG domains exist in *Escherichia coli* PBP1b (*Ec*PBP1b) and *Staphylococcus aureus* PBP2.[39,40] Nine α-helices in the TG are organized into two lobes separated by an extended cleft containing the active site, but the *Ab*PBP1a structure shows only the large lobe (Gα1, Gα6, Gα7, Gα8, and Gα9) without the small lobe (Gα2, Gα3, and Gα4), due to intrinsic flexibility and tryptic cleavage. The key residues of *Ec*PBP1b involved in interaction with moenomycin are highly conserved in *Ab*PBP1a (Figure 3A). The interdomain linker is composed of a six-stranded β-sheet and two perpendicular α-helices. The β-sheet is contributed by two strands from the TG domain, two from the interdomain region, and two from the TP domain. The central region of *Ab*PBP1a harbors the TP domain (residue 273−736) and carries the classical signature of the penicilloyl serine transferase superfamily. The active site, including the nucleophilic Ser434, is located between two subdomains termed α and α/β.

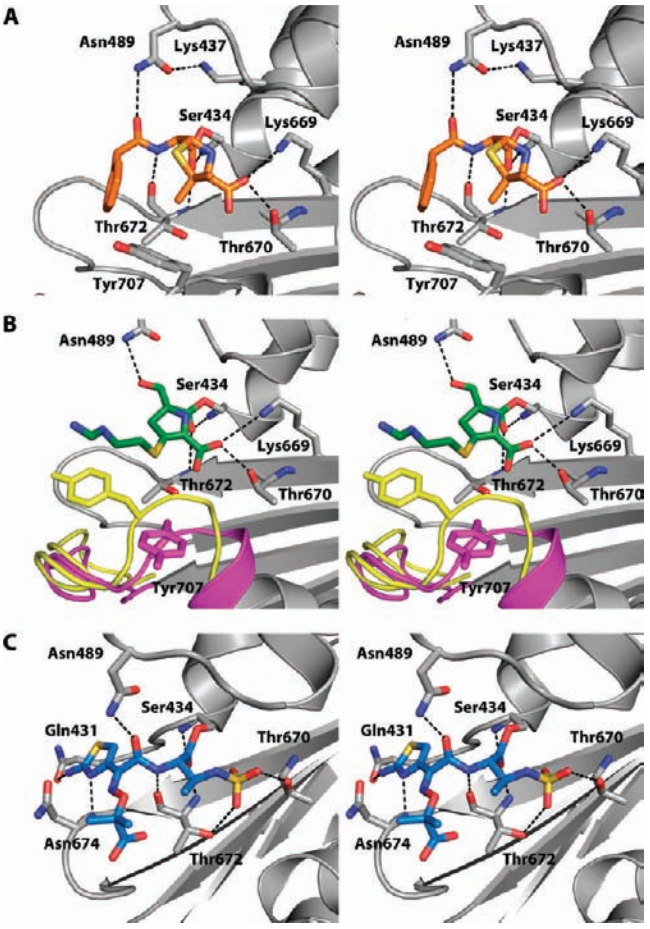

Figure 4. Interactions of Pen G, imipenem, and aztreonam in the active site of the *Ab*PBP1a (stereo). (A) Active site in the benzyl penicillin-acyl *Ab*PBP1a structure. Pen G is shown in stick rendering with orange carbons and hydrogen bonds as dashes. (B) Active site of *Ab*PBP1a bound to imipenem (green). The loop connecting β5 and α11 undergoing significant conformational changes is shown in magenta. The corresponding loop in the apo *Ab*PBP1a structure is shown in yellow. (C) Active site of *Pa*PBP3 bound to aztreonam colored in navy.

The α-subdomain containing α2, α4-α6, and α8 forms one side of the active site groove. The α/β subdomain contains a central core of a five-stranded antiparallel β-sheet (β3/β4/β5/β1/β2) sandwiched by several helices on both sides (α1, α9, α10, and α11) (Figures 3A and S1). Despite low sequence identities, the central five-stranded β-sheet core is highly conserved.

An unexpected feature strongly distinguishes *Ab*PBP1a from the related PBP1b. An additional domain (residues 297−392) containing a five-stranded β-barrel core is inserted in the TP domain between the first α-helix (α1) and the first β-strand (β1) (Figure 3A). A structural similarity search using DALI shows that the β-barrel core structurally resembles translation initiation factor 5A (Z score of 7.0; rmsd of 1.9 Å for 136 Cα atoms) and ribonuclease E (Z score of 6.5; rmsd of 2.8 Å for 80 Cα atoms). Other DALI hits above the threshold (Z = 2.0) include T4 cell puncturing device (Z score of 4.0; rmsd of 3.7 Å for 129 Cα atoms) and pertussis toxin (Z score of 2.8; rmsd of 3.5 Å for 98 Cα atoms). The overall structure contains an OB (oligonucleotide/oligosaccharide binding)-fold domain which is formed by a five-stranded closed β-barrel and capped by an α-helix located between the third and fourth strands. Although

characterization of the OB domain in *Ab*PBP1a awaits completion, it has been shown that the OB-fold proteins possess three structurally conserved loops with ligand-binding properties (these connect secondary structure elements Oβ1 and Oβ2, Oα1 and Oα2, and Oβ5 and Oβ6, respectively) (Figure S1).[41] *Ab*PBP1a is the first example of a multimodular PBP containing the OB-fold domain. Structure-based sequence alignment suggests that this OB-fold domain may also exist in high molecular mass PBPs of subclass A1 from other Gram-negative bacteria including the respective PBP1a proteins of *P. aeruginosa* and *K. pneumoniae* (Figure S1).

Complexes of *Ab*PBP1a with Pen G, Imipenem and Aztreonam. The 2.6 Å resolution crystal structure of Pen-G-treated *Ab*PBP1a includes Pen G covalently bound to Ser434 in the active site of the TP domain (Figure 4A). The carbonyl oxygen of the enzyme−Pen G ester is directed into the oxyanion hole and forms hydrogen bonds with the main chain amides of Ser434 and Thr672. The Pen G carboxylate is anchored by hydrogen bonds with the side chains of Lys669 and Thr670 in the KTGT motif. Lys437 in the conserved SxxK motif is positioned to interact with Asn489 in the SxN motif (Figure S1). The amide bond of Pen G is wedged between the Thr672 backbone carbonyl and the Asn489 side chain. Importantly, the Tyr707 side chain blocking the benzyl binding site in the apo structure is displaced by approximately 6.1 Å toward the solvent-exposed surface when the enzyme is complexed with Pen G, interacting with the Pen G *gem*-dimethyl group and allowing van der Waals interaction with the benzyl group.

Imipenem-treated *Ab*PBP1a was also shown to contain the antibiotic covalently linked to Ser 434. Hydrogen-bonding between the imipenem carboxylate and the KTGT motif resembles that in the Pen G complex, while the C6 ethyl hydroxyl group is hydrogen bonded to Asn489. Electron density beyond the thioether sulfur atom is weak and discontinuous, suggesting that the C2 side chain is flexible and does not interact strongly with the protein. In the imipenem structure, formation of the complex is accompanied by substantial conformational change in the loop connecting β4 and α11 at the mouth of the active site. The Cα atoms of Tyr707 and Gly708 are displaced by 2.4 and 3.8 Å, respectively, away from the active site pocket compared to their positions in the apo structure (Figure 4B).

The crystal structure of aztreonam-linked *Ab*PBP1a reveals that its sulfonic acid group, which activates the β-lactam, is stabilized by Thr670 and Thr672 in the KTGT motif (Figure 4C). The C4 methyl group, which stabilizes the core ring to β-lactamase attack,[42] points into solvent-exposed space. The bulky aminothiazole-containing group is stabilized in the preformed pocket, forming hydrogen bonds with the Gln431 side chain and the Asn674 backbone amide. Electron density for the carboxyl group is weak and shows no strong interaction with *Ab*PBP1a (Figure 5). This is quite different from the complex of aztreonam with the class B enzyme PBP3 of *P. aeruginosa*, in which extensive interactions between the aminothiazole-containing moiety and the target include induced-fit conformational changes of Tyr residues flanked by two highly flexible glycines.[27] Thr528, the corresponding residue in *Ab*PBP1a, accommodates the aminothiazole without rearrangement. In addition, a distinctive aromatic wall composed of residues Tyr, Tyr, and Phe that interacts with the *gem*-dimethyl group in *Pa*PBP3 and accounts for some of the effectiveness of aztreonam against that target is not observed in *Ab*PBP1a.

Complex of *Ab*PBP1a with Monocarbam Siderophore Conjugate MC-1. Crystal structures of *Ab*PBP1a with Pen G, imipenem, and aztreonam were next compared with its structure when complexed with the Trojan Horse monocarbam MC-1 (Figure 6A). MC-1 is composed of a monocyclic β-lactam with a carbonylaminosulfonyl activating group at the N-1 position and a hydroxypyridone siderophore connected by a triazolone-derived linker (Scheme 1). In the conjugate structure with *Ab*PBP1a, the carbonylaminosulfonyl group is anchored by the same residues (Thr670 and Thr672) that interact with the sulfonyl group of aztreonam, but the increased bulk contributed by the carbonylamino function displaces the aminothiazole-containing moiety to outside the active site by 1.4 Å. Despite this, it maintains the hydrogen bond network with Asn674 and Gln431 detected in the aztreonam complex.

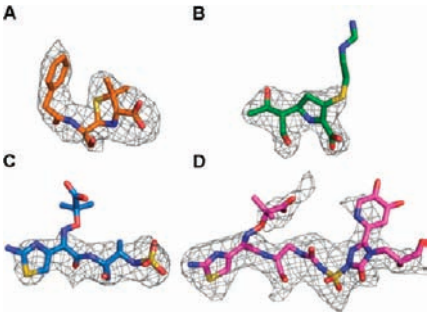

Figure 5. ($F_o - F_c$) omit maps, contoured at 3σ (A) benzyl penicillin colored in orange, (B) imipenem in green, (C) aztreonam in navy, and (D) MC-1 in magenta.

With MC-1 bound, the loop containing residues 707−709 undergoes significant conformational change to extend α-helix 11 further over the triazolone carbonyl group, effectively stabilizing a helix dipole at the N-terminal end of the α11 helix by forming a hydrogen bond interaction with the backbone amide of Gly709. Reorientation of the Tyr707 side chain forms a stacking interaction with the hydroxypyridone siderophore. The structure−activity relationships (SARs) of the monocarbams suggest that the triazolone side chain is tolerant to various sizes and polar functionalities such as an alcohol and amines against *P. aeruginosa* and *A. baumanni*.[19] This flexibility in the SAR is accommodated by the *Ab*PBP1a crystal structures, in which the triazolone side chain generally binds at the mouth of a large pocket formed by two helices (α10a and α11) within which there is sufficient room to accommodate a large side chain (Figure 6A).

Class B *Ab*PBP3 Structure and Active Site Comparison with Class A *Ab*PBP1a. *Ab*PBP3 consists of two domains, an N-terminal non-penicillin-binding domain and a C-terminal TP domain (Figure 3B). The N-terminal domain, unique to high-molecular weight PBPs of subclass B3, extends with several long β-strands and is required for folding and stability of the C-terminal transpeptidase domain. Residues 97−185 in the N-terminal domain are disordered and not visible in the electron density map. The C-terminal domain (residues 266−609) is similar to other TP domains of PBPs, containing a central antiparallel β-sheet composed of five strands (β2/β1/β5/β4/β3). The TP domain of *Ab*PBP3 can be superimposed onto the *Pa*PBP3 TP domain with an rmsd of 0.9 Å for 279 Cα atoms. The active site, including the nucleophilic Ser336, is located in a long cleft running along the β3 strand of the TP domain (Figure 6B).

The *Ab*PBP3 crystal structure possesses a distinctive active site feature also seen in the *Pa*PBP3 structure.[27] In the apo-*Ab*PBP3 crystal structure, the Tyr450 side chain is stabilized by hydrogen

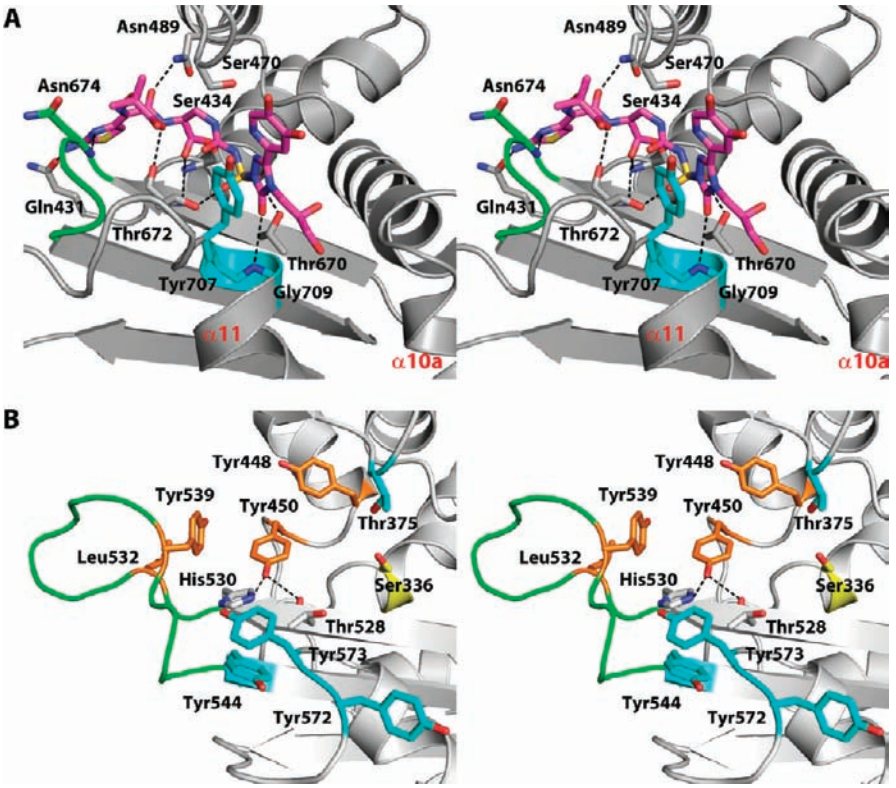

Figure 6. Siderophore-conjugated monocarbam, MC-1, bound to *Ab*PBP1a, and comparison of the structure with apo-*Ab*PBP3 (stereo). (A) Active site in MC-1-acyl-*Ab*PBP1a complex. MC-1 is shown in stick rendering with magenta carbons. The short loop connecting β3 and β4 is shown in green and the extended α-helix (residue 707−709) upon MC-1 binding in cyan. (B) Active site of apo-*Ab*PBP3. The catalytic Ser336 is shown in yellow. The residues involved in hydrophobic interaction are shown in orange. Residues with the potential to form an aromatic wall upon monocarbam binding are shown in cyan. The extended loop connecting β3 and β4 (residue 531−544) is shown in green.

bonds with the Thr528 and His530 backbone amides, blocking the binding site for aminothiazole-containing β-lactams. Tyr450 is flanked by two highly flexible glycyl residues and participates in conformational changes induced by the binding of aminothiazole moieties. As seen in the recent MC-1-*Pa*PBP3 crystal structure, *Ab*PBP3 has conserved residues (Tyr572, Tyr573, and Tyr544) that could form an aromatic wall to play a similar role for interaction with the *gem*-dimethyl group of MC-1. Despite this, the entrance to the active site cleft of *Ab*PBP3 differs significantly from that of *Pa*PBP3. Two polar residues, Thr375 and Tyr573, are located at the central portion of the *Ab*PBP3 active site and are positioned to interact with β-lactam inhibitors. In *Pa*PBP3, direct hydrophobic interaction of Val333 and Phe533 creates a tunnel-like hydrophobic barrier to restrict access to the cleft.

Certain striking differences exist between the active sites of *Ab*PBP3 and *Ab*PBP1a. In *Ab*PBP3, an extended loop that connects β3 and β4 (residues 531−544) widens the active-site cleft at one end, whereas the shorter loop formed by residues 674−676 of *Ab*PBP1a makes the active site cleft comparatively narrow (Figure 6A,B). In the apo-*Ab*PBP3 crystal structure, Leu532 and Tyr539 in the loop connecting β3 and β4 form a hydrophobic pocket with Tyr450 and Tyr448. Upon binding of bulky aminothiazole-containing ligands such as MC-1 and aztreonam, significant conformational changes are likely to allow the Tyr450 side chain to swing out toward the solvent-exposed surface, reshaping the hydrophobic pocket that involves the β3-β4 connecting loop. The β3-β4 interconnecting region is flexible with poor sequence conservation among PBPs, and its flexibility has been proposed as a critical factor governing substrate binding and release. Furthermore, mutations in drug-resistant strains involve the β3-β4 interconnecting loop that contributes to different specificities and affinities of β-lactam analogues across PBPs.[43]

Thermal Stability (T_m) and Solvent Rearrangement Effects. It would clearly be of interest to measure the equilibrium affinity of β-lactam antibiotics for their PBP targets in isolation from other parameters, but this is made difficult by the rapid conversion of their first productive collision complex into covalent adducts. An accessible surrogate measurement is assessment of the difference in stability between a free receptor and its complex with a ligand,[44,45] or in this case between a free PBP and its covalent complex. (It must be acknowledged that rearrangements are possible after the covalent step has occurred, as can also occur with noncovalent ligand−receptor associations.)

As a biophysical counterpart to structural studies of *Ab*PBP1a, thermal shift assays were performed to gauge thermodynamic stabilization or destabilization of *Ab*PBP1a by covalent agents. An increase in T_m relative to apo-*Ab*PBP1a (T_m of 47 °C) indicated that a covalent adduct acquired extra stability. MC-1 binding significantly increased T_m, but imipenem did not (Table 2). The T_m values generated were not converted into thermodynamic values, as they were not derived from reversible denaturation events.

Studies by Shoichet et al.[46−49] employed reversible thermal denaturation experiments with the β-lactamase TEM-1 and PBP5 of *E. coli* to demonstrate a lack of correlation between second-order rate constants for acylation that are indicative of the

potencies of covalent inhibitors and the noncovalent interaction energies often used in structure-based design. In the case of imipenem, it was reasoned (on the basis of earlier crystal structures with TEM-1[50]) that a steric clash between Asn132 and the 6α-1*R*-hydroxyethyl substituent caused an unprecedented "flipped out" conformation of the carbonyl oxygen of the β-lactam ring in the oxyanion pocket, destabilizing the TEM-1 complex. Consistent with this, imipenem *stabilized* the N132A TEM-1 mutant.

The impienem-*Ab*PBP1A crystal structure reported here did not exhibit the "flipped out" carbonyl oxygen, and Asn489 of *Ab*PBP1a (equivalent to Asn132 of TEM-1) had very similar conformations in both the MC-1 and imipenem structures. Most of the oxyanion interactions were also similar, suggesting that the effect of the 6α-1*R*-hydroxyethyl substituent was not dominant in this case. Conformational changes outside the oxyanion hole, as in Asn674, Ser470, and Lys669, are attributed to other structural differences between MC-1 and imipenem, such as the presence of the *gem*-dimethyl-carboxylate-moiety and sulfonyl urea in MC-1.

These data led us to hypothesize that solvent rearrangement effects during ligand binding impacted both the potencies of these compounds and the thermal stabilities of their respective covalent adducts, providing an alternative explanation for the observed differences in thermal stability. As ligand binding involves the exchange of protein-to-water for protein-to-ligand contacts, dissection of the thermodynamics of hydration sites and the displacement of waters upon ligand binding could provide insight into the thermal stability of the protein—ligand complex. To investigate the effects of protein desolvation energies, WaterMap[32] was used to compute the thermodynamic profile and free energies of hydration sites in *Ab*PBP1a in several structures relative to bulk solvent. As previously reported, the WaterMap energies[27,29,30] approximate free energy based exclusively on the displacement of water molecules within the ligand binding site and ignore other terms such as protein—ligand van der Waals contacts, electrostatic interactions, internal strain of ligand or protein, and conformational effects. The rank order of thermal stability data paralleled the order that emerged from calculating WaterMap energies, with MC-1 and Pen G showing significant protein desolvation effects that stabilized their *Ab*PBP1a—ligand complexes relative to those with aztreonam and imipenem (Table 2). Therefore, although these ligands showed considerable structural variation both in their core lactam moieties and in their side-chains, the total desolvation energies provided by WaterMap appeared to be valid indicators of the relative thermal stabilities of their covalent adducts with *Ab*PBP1a. This result provided an additional perspective on the observed differences in thermal stability among a range of receptor—ligand complexes.

Table 2. Biophysical Characterization of β-Lactam Interactions with *Ab*PBP1a

		WaterMap energies (kcal/mol)		
compd	thermal stability T_m[a] (°C)	ΔH	$-T\Delta S$	ΔG
imipenem	47	−15.2	8.0	−7.2
Pen G	54	−20.1	1.6	−18.5
aztreonam	50	−14.5	3.8	−10.7
MC-1	56	−35.7	6.9	−28.8

[a] T_m: thermal stability (apo *Ab*PBP1*a* = 47 °C).

Structure-Based Design of Agents To Treat Infections with *A. baumanii*. In this study, the two objectives have been to rationalize the respective activities of standard β-lactams against the emerging pathogen *A. baumannii*, and to observe the performance (with a view to further improvement) of the Trojan Horse agent MC-1.

When the crystal structures of *Ab*PBP1a and *Ab*PBP3 were compared with structures of their orthologs from *P. aeruginosa*, distinctive features of the *A. baumannii* proteins could be detected. First, a hydrophobic aromatic wall formed by Phe-Tyr-Tyr residues in *Pa*PBP3 is absent in *Ab*PBP1a; this structural feature of *Pa*PBP3 was crucial in local conformational changes that narrowed the substrate binding site and excluded water molecules during MC-1 binding. Second, Arg489 of *Pa*PBP3, which forms a crucial salt bridge to the *gem*-dimethyl carboxylic acid, is substituted by His530 in *Ab*PBP1a and by Asn674 in *Ab*PBP3. His530 of *Ab*PBP1a is located at the bottom of the pocket and does not form a productive salt bridge interaction. Also, the constraint imposed by the *gem*-dimethyl functional group precludes the ligand from adopting a conformation that permits a reasonable interaction with His530. Third, Tyr409 that adopts an "in" conformation in the apo structure and opens into an "out" conformation upon the aminothiazole side chain binding in the *Pseudomonas* PBPs is Thr528 in *Ab*PBP1a and Tyr450 in *Ab*PBP3. The crystal structure indicates that a key bifurcated H-bond formed between the amine of the aminothiazole and Glu291 carboxylic acid and backbone carbonyl of Arg489 in the *Pseudomonas* structure is not observed and not possible in *Ab*PBP1a (the amino group forms a single hydrogen bond to Gln431), reducing the importance of the aminothiazole group for activity. Furthermore, from the list of compounds profiled it appears that potentially better acylation rates and better MIC profiles can be achieved by modifying the side of the molecule placed on the left in Figure 7. Collectively, these structural insights, hypotheses, and biophysical data suggest that the next generation

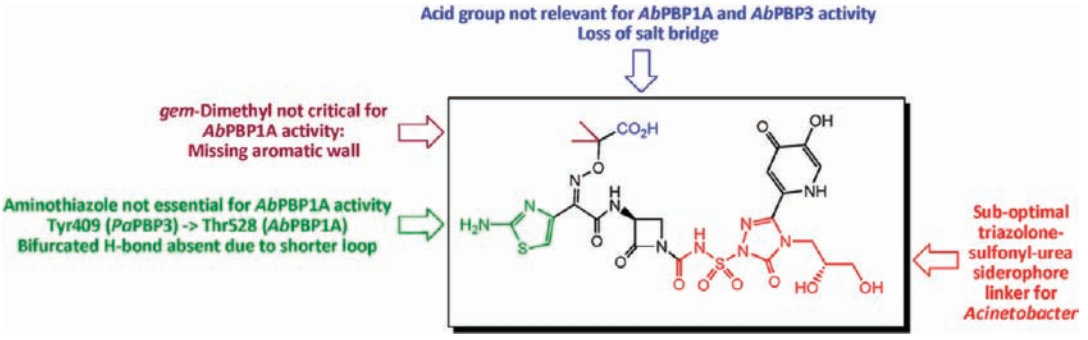

Figure 7. *Acinetobacter baumanii* PBP inhibitor design strategies.

of β-lactams can be further optimized for *Acinetobacter* through modifications primarily to this side of the molecule.

CONCLUSION

Structures of *Ab*PBP1a covalently linked with Pen G, imipenem, aztreonam, and a siderophore-conjugated triazolone-linked monocarbam have been aligned with biophysical and computational analyses to rationalize the activities of a representative set of β-lactams against this key target protein in an increasingly significant Gram-negative pathogen. In the course of this work, a previously unknown domain was recognized that represents a distinct feature of the high-molecular-weight class A PBP subfamily in *Acinetobacter*. The study has been broadened by additional data with *Ab*PBP3, which is also part of the PBP target in *A. baumannii*. Structural, biophysical, and computational characterization of covalently bound β-lactams and novel siderophore-conjugated monocarbams to *A. baumannii* PBPs provide a much needed paradigm shift in the prospective design of more effective antibiotics. These results provide insight and opportunities for improved compound design with a view to enhancing the power of antibacterial action available to combat infections with *A. baumannii*.

ASSOCIATED CONTENT

Supporting Information. Complete refs 4 and 19. Additional figure and table. This material is available free of charge via the Internet at http://pubs.acs.org.

AUTHOR INFORMATION

Corresponding Author
seungil.han@pfizer.com

ACKNOWLEDGMENT

We thank Lisa Aschenbrenner for determining MIC, Viva Biotech Ltd. in China for technical support, James Wasicak, Michael Dixon, Matthew Brown, Mark Plummer, John Mueller, Xiayang Qiu, and Mark Noe for insightful discussions, and the anonymous reviewers for their critical feedback and knowledgeable observations.

REFERENCES

(1) Coates, A. R. M.; Halls, G.; Hu, Y. *Br. J. Pharmacol.* **2011**, *163*, 184–194.
(2) Boucher, H. W.; Talbot, G. H.; Bradley, J. S.; Edwards, J. E.; Gilbert, D.; Rice, L. B.; Scheld, M.; Spellberg, B.; Bartlett, J. *Clin. Infect. Dis.* **2009**, *48*, 1–12.
(3) Spellberg, B.; Guidos, R.; Gilbert, D.; Bradley, J.; Boucher, H. W.; Scheld, W. M.; Bartlett, J. G.; Edwards, J., Jr. *Clin. Infect. Dis.* **2008**, *46*, 155–64.
(4) Livermore, D. M.; et al. *J. Antimicrob. Chemother.* **2011**, *66*, 1941–1944.
(5) Giamarellou, H.; Poulakou, G. *Drugs* **2009**, *69*, 1879–1901.
(6) Lortholary, O.; Fagon, J. Y.; Hoi, A. B.; Slama, M. A.; Pierre, J.; Giral, P.; Rosenzweig, R.; Gutmann, L.; Safar, M.; Acar, J. *Clin. Infect. Dis.* **1995**, *20*, 790–6.
(7) Meric, M.; Kasap, M.; Gacar, G.; Budak, F.; Dundar, D.; Kolayli, F.; Eroglu, C.; Vahaboglu, H. *FEMS Microbiol. Lett.* **2008**, *282*, 214–218.
(8) Gootz, T. D.; Marra, A. *Expert Rev. Anti-Infect. Ther.* **2008**, *6*, 309–325.
(9) Ghuysen, J. M. *Annu. Rev. Microbiol.* **1991**, *45*, 37–67.
(10) Cuenca, F. F.; Pascual, A.; Martinez Marinez, L.; Conejo, M. C.; Perea, E. J. *J. Basic Microbiol.* **2003**, *43*, 194–201.
(11) Vashist, J.; Tiwari, V.; Das, R.; Kapil, A.; Rajeswari, M. R. *Indian J. Med. Res.* **2011**, *133*, 332–338.
(12) Eijkelkamp, B. A.; Hassan, K. A.; Paulsen, I. T.; Brown, M. H. *BMC Genomics* **2011**, *12*, 126.
(13) Zimbler, D. L.; Penwell, W. F.; Gaddy, J. A.; Menke, S. M.; Tomaras, A. P.; Connerly, P. L.; Actis, L. A. *BioMetals* **2009**, *22*, 23–32.
(14) Budzikiewicz, H. *Curr. Top. Med. Chem.* **2001**, *1*, 73–82.
(15) Cornelis, P. *Appl. Microbiol. Biotechnol.* **2010**, *86*, 1637–1645.
(16) Miethke, M.; Marahiel, M. A. *Microbiol. Mol. Biol. Rev.* **2007**, *71*, 413–451.
(17) Möllmann, U.; Heinisch, L.; Bauernfeind, A.; Köhler, T.; Ankel-Fuchs, D. *BioMetals* **2009**, *22*, 615–624.
(18) Page, M. G. P.; Dantier, C.; Desarbre, E. *Antimicrob. Agents Chemother.* **2010**, *54*, 2291–2302.
(19) Flanagan, M. E.; et al. *ACS Med. Chem. Lett.* **2011**, *2*, 385–390.
(20) Otwinowski, Z.; Minor, W. *Methods Enzymol.* **1997**, *276*, 307–326.
(21) Vonrhein, C.; Blanc, E.; Roversi, P.; Bricogne, G. *Methods Mol. Biol.* **2007**, *364*, 215–230.
(22) Perrakis, A.; Morris, R.; Lamzin, V. S. *Nat. Struct. Biol.* **1999**, *6*, 458–63.
(23) Emsley, P.; Cowtan, K. *Acta Crystallogr., Sect. D: Biol. Crystallogr.* **2004**, *60*, 2126–2132.
(24) Blanc, E.; Roversi, P.; Vonrhein, C.; Flensburg, C.; Lea, S. M.; Bricogne, G. *Acta Crystallogr., Sect. D: Biol. Crystallogr.* **2004**, *60*, 2210–21.
(25) McCoy, A. J.; Grosse-Kunstleve, R. W.; Adams, P. D.; Winn, M. D.; Storoni, L. C.; Read, R. J. *J. Appl. Crystallogr.* **2007**, *40*, 658–674.
(26) Laskowski, R. A.; Moss, D. S.; Thornton, J. M. *J. Mol. Biol.* **1993**, *231*, 1049–1067.
(27) Han, S.; Zaniewski, R. P.; Marr, E. S.; Lacey, B. M.; Tomaras, A. P.; Evdokimov, A.; Miller, J. R.; Shanmugasundaram, V. *Proc. Natl. Acad. Sci. U.S.A.* **2010**, *107*, 22002–22007.
(28) Rajamohan, F.; Harris, M. S.; Frisbie, R. K.; Hoth, L. R.; Geoghegan, K. F.; Valentine, J. J.; Reyes, A. R.; Landro, J. A.; Qiu, X.; Kurumbail, R. G. *Protein Expression Purif.* **2010**, *73*, 189–197.
(29) Abel, R.; Young, T.; Farid, R.; Berne, B. J.; Friesner, R. A. *J. Am. Chem. Soc.* **2008**, *130*, 2817–2831.
(30) Beuming, T.; Farid, R.; Sherman, W. *Protein Sci.* **2009**, *18*, 1609–1619.
(31) Robinson, D. D.; Sherman, W.; Farid, R. *ChemMedChem* **2010**, *5*, 618–627.
(32) Young, T.; Abel, R.; Kim, B.; Berne, B. J.; Friesner, R. A. *Proc. Natl. Acad. Sci. U.S.A.* **2007**, *104*, 808–813.
(33) Bowers, K. J.; Chow, E.; Xu, H.; Dror, R. O.; Eastwood, M. P.; Gregersen, B. A.; Klepeis, J. L.; Kolossvary, I.; Moraes, M. A.; Sacerdoti, F. D.; Salmon, J. K.; Shan, Y.; Shaw, D. E. In *Proceedings of the ACM/IEEE Conference on Supercomputing (SC06)*; ACM Press: New York, 2006.
(34) Jorgensen, W. L.; Maxwell, D. S.; Tirado-Rives, J. *J. Am. Chem. Soc.* **1996**, *118*, 11225–11236.
(35) Kaminski, G. A.; Friesner, R. A.; Tirado-Rives, J.; Jorgensen, W. L. *J. Phys. Chem. B* **2001**, *105*, 6474–6487.
(36) Lee, V. J.; Miller, G. H.; Yagisawa, M. *Curr. Opin. Microbiol.* **1999**, *2*, 475–482.
(37) Quinn, J. P. *Diagn. Microbiol. Infect. Dis.* **1998**, *31*, 389–395.
(38) Sykes, R. B.; Bonner, D. P.; Bush, K.; Georgopapadakou, N. H. *Antimicrob. Agents Chemother.* **1982**, *21*, 85–92.
(39) Lovering, A. L.; de Castro, L. H.; Lim, D.; Strynadka, N. C. *Science* **2007**, *315*, 1402–1405.
(40) Sung, M. T.; Lai, Y. T.; Huang, C. Y.; Chou, L. Y.; Shih, H. W.; Cheng, W. C.; Wong, C. H.; Ma, C. *Proc. Natl. Acad. Sci. U.S.A.* **2009**, *106*, 8824–8829.
(41) Agrawal, V.; Kishan, K. V. *Curr. Protein Pept. Sci.* **2003**, *4*, 195–206.
(42) Miller, M. J. *Chem. Rev.* **1989**, *89*, 1563–1579.
(43) Contreras-Martel, C.; Dahout-Gonzalez, C.; Martins Ados, S.; Kotnik, M.; Dessen, A. *J. Mol. Biol.* **2009**, *387*, 899–909.

(44) Morton, A.; Matthews, B. W. *Biochemistry* **1995**, *34*, 8576–8588.
(45) Schellman, J. A. *Biopolymers* **1976**, *15*, 999–1000.
(46) Beadle, B. M.; McGovern, S. L.; Patera, A.; Shoichet, B. K. *Protein Sci.* **1999**, *8*, 1816–1824.
(47) Beadle, B. M.; Nicholas, R. A.; Shoichet, B. K. *Protein Sci.* **2001**, *10*, 1254–1259.
(48) Beadle, B. M.; Shoichet, B. K. *Antimicrob. Agents Chemother.* **2002**, *46*, 3978–3980.
(49) Wang, X.; Minasov, G.; Shoichet, B. K. *Proteins: Struct., Funct., Genet.* **2002**, *47*, 86–96.
(50) Maveyraud, L.; Mourey, L.; Kotra, L. P.; Pedelacq, J.-D.; Guillet, V.; Mobashery, S.; Samama, J.-P. *J. Am. Chem. Soc.* **1998**, *120*, 9748–9752.